Tracking Control of Oscillatory Motion in IPMC Actuators for Underwater Applications

Sisi Song[1], Yingfeng Shan[1], Kwang J. Kim[2,†] and Kam K. Leang[1,‡]

[1]Electroactive Systems and Controls Laboratory
[2]Active Materials and Processing Laboratory
Department of Mechanical Engineering
University of Nevada-Reno
Reno, Nevada 89557-0312, USA

Abstract*— Ionic polymer-metal composite (IPMC) actuators have many advantages; for instance, they (1) can be driven with low voltages (<5 V); (2) are soft, flexible and easily shaped; and (3) can operate in an aqueous environment (such as water). Important applications for IPMCs include active catheter devices for minimally invasive surgery, artificial muscle, and sensors and actuators for biorobotics. For applications such as endoscopy and flapping-based propulsion systems in aquatic robots, the IPMC actuator is required to precisely track a periodic reference trajectory. However, due to dynamic effects, nonlinear behavior, and external disturbances, uncompensated open-loop control yields excessively-large tracking error. This paper focuses on precision tracking of oscillatory motion in IPMC actuators. A feedback controller based on the repetitive control concept is proposed to improve tracking performance from one operating period to the next. The stability of the controller is analyzed in the discrete-time domain, and design considerations are discussed. The method is applied to a newly fabricated Perfluorinated Ion Exchange Membrane based IPMC actuator with lithium as its counter-ion. The tip displacement of the IPMC actuator is measured by a strain gage sensor. This newly proposed sensing scheme is low cost, practical, effective, and importantly, compact. Experimental results show the combined control and sensing scheme can minimize the tracking error by approximately 50% compared to PID control for tracking of periodic signals including sinusoidal and triangular wave forms.

I. INTRODUCTION

Ionic polymer-metal composites (IPMCs) are innovative materials that can be exploited for emerging robotic systems and biomedical devices [1]–[4]. Due to their low driving voltage (<5 V), large strain, soft and flexible structure, and the ability to operate in an aqueous environment, IPMCs are suited for the development of innovative propulsion systems in underwater autonomous systems [5]–[8]. For example, strips of IPMCs have been used to develop the legs (antennae) of a jellyfish-like robot in [9]. The walking speed of the jellyfish was controlled by the frequency of the input voltage applied to the IPMC legs. Likewise, the caudal fin to propel a robotic fish was created from an IPMC actuator in [10]. The achievable peak swimming speed of the robotic fish is 6.6 mm/s for an actuation frequency of 2 Hz. Additionally, IPMC actuators can play a critical role in the development of innovative highly-maneuverable biorobotic vehicles, *e.g.*, [11]. The application of IPMC actuators for propulsion and maneuvering in underwater systems often require the actuator to exhibit oscillatory motion. For instance, the movement of the IPMC-based caudal fin and the scanning motion of an IPMC-based active endoscope are periodic in time. In the former case, precision tracking of the oscillatory motion is needed for predictable and accurate maneuvering [12]. The contribution of this article is the development and application of a repetitive controller for IPMCs for precision tracking of oscillatory motion. The feedback sensing signal is made possible by integrating a strain gage sensor with the IPMC actuator. This new approach to sensing the motion of the IMPC is chosen because of its simplicity, low cost, and compactness. These sensors can also be embedded within the IPMC material to create an integrated sensor/actuator system. It is pointed out that the proposed control approach is also applicable with other sensing methods, *e.g.*, [13], [14].

Recent work on control approaches for IPMCs comprise of feedback-based approaches and open-loop feedforward methods to minimize or compensate for dynamic and nonlinear effects. Integrated feedback and feedforward control has also been investigated [15]. Proportional-integral-derivative (PID) feedback control has been applied to IPMC [3]. Likewise, the adaptive control method has been investigated for IPMC subjected to noise and changes in relative humidity level [16]. A model-reference controller for IPMC was investigated in [17] to account for the drift effect. The controller was based on a fourth-order empirical model; however, similar results were obtained using a lower second-order model. The linear parameter varying approach was applied to control an IPMC actuator in [18] for active catheter systems. Integrated IPMC actuator and PVDF sensor was explored for feedback control in [19]. Existing control methods, such as PID, offer acceptable tracking performance; however, for tracking of oscillatory reference trajectories, the tracking error may still be unacceptably large.

The contribution of this work is the development of a discrete-time repetitive controller (RC) for precision tracking

Authors gratefully acknowledge support from the Office of Naval Research, grant number N000140910218.

†E-mail: kwangkim@unr.edu.
‡Corresponding author; E-mail: kam@unr.edu.

of periodic reference trajectories for IPMC. The RC approach is well-suited in applications that include IPMC-based underwater propulsion systems where the actuator's motion is required to be periodic in time. In general, most applications that require the IPMC to move in a periodic fashion can also benefit from RC. For practical implementation, a strain gage sensor is proposed for providing feedback information to the controller. The sensor is integrated with the IPMC actuator to create a compact actuator/sensor system and the relationship between strain and actuator displacement is presented. Therefore, sensors such as lasers which can be sensitive to surface reflectivity are not required for feedback control.

II. CONTROLLER DESIGN

Repetitive control is well suited for tracking periodic trajectories [20], [21]. The control structure is based on the internal model principle. Compared to traditional proportional-integral (PI) or PID feedback controllers [3], where careful tuning is required and the residual tracking error persists from one operating cycle to the next, RC has the ability to reduce the error as the number of operating cycles increases [22]. The key feature of RC is a signal generator within the feedback loop (see Fig. 1) — the signal generator provides infinite gain at the fundamental frequency of the reference trajectory and its harmonics [20].

Let $R(z)$ be the z-transform of a given periodic reference trajectory with period T_p. The pure delay z^{-N} within the inner positive feedback loop creates a signal generator, where $N = T_p/T_s$ and T_s is the sampling period. It is pointed out that RC can also be 'plugged into' to an existing feedback controller to enhance tracking of periodic trajectories.

It is assumed that the input-output dynamics of the IPMC actuator is linear and represented by $G(z)$, where $z = e^{j\omega T_s}$, for $\omega \ \epsilon \ (0, \pi/T_s)$. The low-pass filter for robustness is denoted by $Q(z)$ and $P(z) = z^m$ (where m is a non-negative integer) is a positive phase-lead compensator to enhance the performance of the RC feedback system. Specifically, $P(z)$ provides $\theta(j\omega) = mT_s$ lead in phase.

By inspection, the transfer function of the signal generator

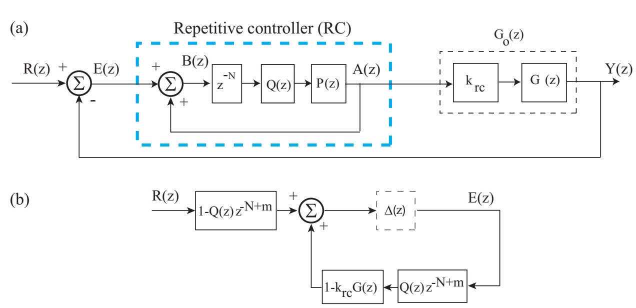

Fig. 1. (a) The block diagram of repetitive control system where the reference and output trajectories are $R(z)$ and $Y(z)$, respectively. The RC consists of a pure delay z^{-N}, low-pass filter $Q(z)$ for robustness, and a linear phase lead $P(z)$ to enhance performance. (b) Equivalent system for stability analysis.

that relates the signals $E(z)$ to $A(z)$ in Fig. 1 is given by

$$\frac{A(z)}{E(z)} = \frac{Q(z)P(z)z^{-N}}{1 - Q(z)P(z)z^{-N}} = \frac{Q(z)z^{(-N+m)}}{1 - Q(z)z^{(-N+m)}}. \quad (1)$$

Without the low-pass filter $Q(z)$ and positive phase lead compensator $P(z)$, the poles of the signal generator are $1 - z^{-N} = 0$. Therefore, the RC controller provides infinite gain at the harmonics of the periodic reference trajectory for tracking periodic trajectories. One drawback, however, is the large gain of RC at high frequencies can lead to instability of the closed-loop system. Therefore, practical RC design incorporates a low-pass filter $Q(z)$ to address the stability and robustness issues. For simplicity, a low-pass filter of the form $Q(z) = \frac{a}{z+b}$, where $|a| + |b| = 1$, is chosen. Alternatively, the following zero-phase filter can also be considered [23]:

$$Q(z, z^{-1})_n = \sum_{i=0}^{n} b_i z^i + \sum_{i=1}^{n} b_i z^{-i}, \quad (2)$$

where $0 < b_i < 1$, and $\sum_{i=0}^{n} b_i + \sum_{i=1}^{n} b_i = 1$.

Achieving a stable closed-loop is one of the main challenges of RC. Let $H(z) = Q(z)z^{(-N+m)}$ and $G_0(z) = k_{rc}G(z)$, where k_{rc} is referred to as the RC gain. It is assumed that the reference trajectory $R(z)$ is periodic in time, and thus has a discrete frequency spectrum.

The transfer function relating the reference trajectory $R(z)$ and the tracking error $E(z)$ is

$$S_{rc}(z) = \frac{E(z)}{R(z)} = \frac{1 - H(z)}{1 - H(z)[1 - G_0(z)]}. \quad (3)$$

Using Eq. (3), the RC block diagram in Fig. 1(a) is simplified to the equivalent interconnected system shown in Fig. 1(b). Replacing $z = e^{j\omega T_s}$, and since $1 - H(z)$ is stable, the positive feedback system in Fig. 1(b) is asymptotically stable by the Small Gain Theorem [24] when

$$|H(z)[1 - G_0(z)]| = |H(e^{j\omega T_s})[1 - k_{rc}G(e^{j\omega T_s})]| < 1, \quad (4)$$

for all $\omega \ \epsilon \ (0, \pi/T_s)$. Noting that $|Q(e^{j\omega T_s})| \leq 1$,

$$|1 - k_{rc}G(e^{j\omega T_s})| < 1 \leq \frac{1}{|Q(e^{j\omega T_s})|}, \quad (5)$$

and setting the transfer function of the IPMC to $G(e^{j\omega T_s}) = A(\omega)e^{j\theta(\omega)}$, where $A(\omega) > 0$ and $\theta(\omega)$ are the magnitude and phase of $G(e^{j\omega T_s})$, respectively, Eq. (4) is simplified to

$$|1 - k_{rc}A(\omega)e^{j\theta(\omega)}| < 1. \quad (6)$$

Observing that $e^{j\theta} = \cos(\theta) + j\sin(\theta)$ and requiring $k_{rc} > 0$, Eq. (6) gives $1 - 2k_{rc}A(\omega)\cos[\theta(\omega)] + k_{rc}^2 A^2(\omega) < 0$; hence,

$$0 < k_{rc} < 2\cos[\theta(\omega)]/A(\omega). \quad (7)$$

Therefore, by picking a sufficiently small k_{rc}, stability of the closed-loop system is guaranteed. It is noted that the lead compensator $P(z)$ compensates for the phase lag caused by the low-pass filter $Q(z)$, and thus can be used to improve the tracking performance [25]. Because $N >> m$, the modified delay z^{-N+m} is causal and can be easily implemented digitally. Additionally, the RC gain k_{rc} can be adjusted to improve closed-loop robustness and the rate of convergence of the tracking error.

III. The Experimental System

The repetitive controller is implemented on a newly fabricated perfluorinated ion exchange membrane based IPMC actuator with lithium as its counter-ion. The experimental IPMC system, including a new approach for sensing the displacement of the IPMC actuator using a strain gage sensor, is described next.

A. IPMC Manufacturing Process

An electroless plating process is used to manufacture the IPMC actuator [5]. First, a pre-treatment is performed on the ion exchange membrane prior to electroding to eliminate organic and metallic impurities. Basically, the membrane is heated to 80°C in 3% hydrogen peroxide (H_2O_2) and in 15% nitric acid (HNO_3). Next, the membrane is immersed for 3 hours in the platinum complex solution prepared with tetraamineplatinum (II) chloridemonohydrate ($[Pt(NH_3)_4]Cl_2xH_2O$, Aldrich). Subsequently, the membrane is rinsed with de-ionized water. For the initial metalization of the membrane surface with platinum particles, the membrane is reduced in a sodium borohydride ($NaBH_4$, Aldrich) solution for 3 hours. The membrane is additionally run through the platinum electroding process to increase the surface conductivity. Finally, the cation of manufactured IPMC is exchanged to Li^+ by using 1M lithium chloride (LiCl, Aldrich) solution.

The open-loop response of the IPMC actuator to a square-wave input is shown in Fig. 2, measured with a laser displacement sensor (IPMC dimensions $L = 25$ mm, $w = 10$ mm, and $t = 0.5$ mm). The IPMC initially responds quickly by bending to a maximum value, then slowly back-relaxes and reaches an equilibrium position beyond the initial starting position.

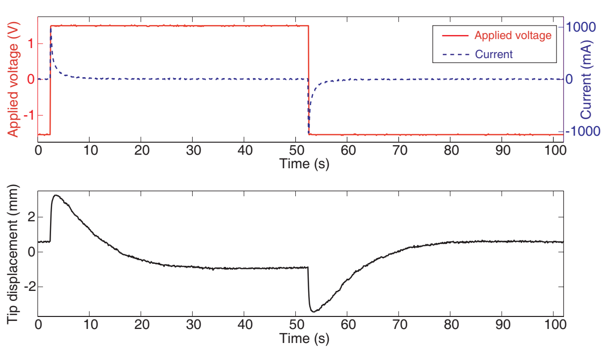

Fig. 2. Open-loop response of Li^+ based IPMC showing back relaxation behavior recorded after 10 cycles (measured with laser sensor).

B. Strain Gage Displacement Sensor

For position control of active material actuators such as piezoelectric actuators, resistive strain gages are commonly used. One of the advantages of strain sensors is they are

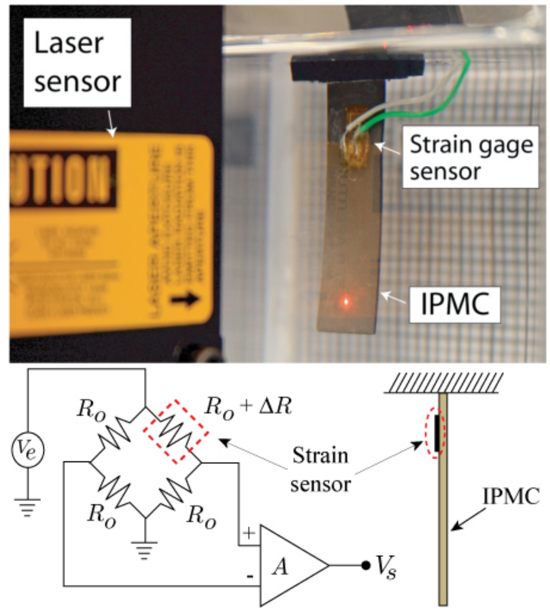

Fig. 3. Strain sensor for IPMC.

compact and can be easily bonded to the surface of an actuator. Resistive strain gage sensors are made of a thin layer of conducting foil sealed between two insulating layers. When the gage is elongated, the resistance changes proportional to strain ϵ by

$$\Delta R = G R_o \epsilon, \tag{8}$$

where R_o is the nominal resistance value of the gage. The gage factor G is a characteristic of the gage.

Figure 3 shows a photograph of a small strain sensor (Omega SGD-3/350-LY13, $R_o = 350\ \Omega$, dimensions of 7×4 mm.) bonded on the surface of the IPMC actuator near its clamped end. The actuator is shown submerged in de-ionized water and a laser is also used to measure the tip displacement. The quarter-bridge circuit shown produces a change in output voltage ΔV as a function of the strain ϵ,

$$\Delta V = \frac{G\epsilon}{4}\left[\frac{1}{1+G\frac{\epsilon}{2}}\right]V_e, \tag{9}$$

where V_e is the excitation voltage. Neglecting the bridge nonlinearity, the output voltage as a function of strain is

$$V_s = AG\epsilon V_e/4, \tag{10}$$

where A is the amplifier gain (*e.g.*, $A = 2000$). Since the achievable strain for an IPMC actuator is between 0.1% to a few percent, the change in resistance of the gage sensor is relatively small and thus the bridge voltage is amplified by a strain-gage amplifier (Vishay model 2120B).

Using the voltage amplifier (see discussion below) to control the IPMC, Figure 4 shows the time response of the measured strain signal ϵ compared to the measured tip displacement acquired using a laser sensor. The results show that the IPMC bending behavior induces a strain which can be measured by the strain gage sensor attached to the surface of the IPMC actuator. In addition, these sensors can be

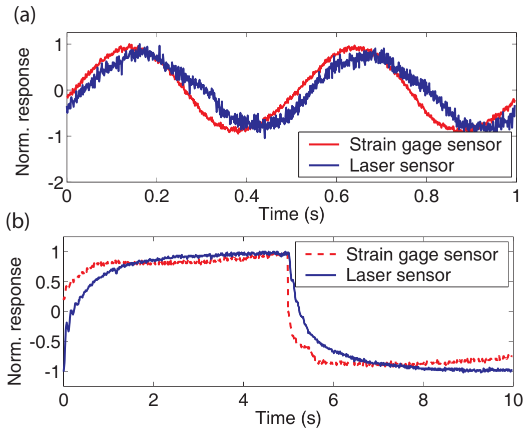

Fig. 4. Comparison between measured strain signal and tip displacement measured by laser sensor for (a) 2 Hz sine wave and (b) 0.1 Hz square wave input.

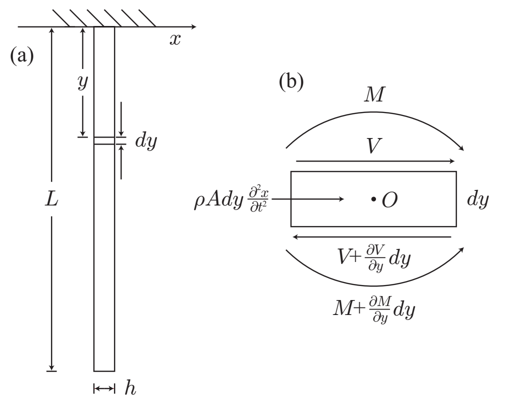

Fig. 5. (a) Cantilever beam. (b) Free-body diagram of beam element.

embedded within the material to create an integrated sensor/actuator system. Multiple sensors appropriately oriented can detect both bending and twisting behavior for sectored-electroded IPMCs [26].

The strain-to-displacement relationship for the IPMC actuator is developed assuming that the IPMC's bending response follows that of a isotropic cantilever beam shown in Fig. 5(a) [27]. Let $x(y,t)$ denote the displacement from the neutral axis of a segment [Fig. 5(b)] of the beam located at the distance y from the fixed end. The objective is to determine the transverse displacement $x(y,t)$ given a strain measurement $\epsilon(y,t)$. The displacement will then be used for feedback control.

For the cantilever beam shown in Fig. 5(a), it is assumed that the following general equation of motion holds

$$\rho A \frac{\partial^2 x(y,t)}{\partial t^2} + c(y)\frac{\partial x(y,t)}{\partial t} + EI\frac{\partial^4 x(y,t)}{\partial y^4} = F(y,t), \quad (11)$$

where ρ is the density, A is the cross-sectional area, E is the Young's modulus, I is the moment of inertia, and $c(x)$ and $F(y,t)$ are the damping coefficient and applied load per unit length, respectively.

The solution to the equation of motion (11) is obtained by separating $x(y,t)$ into two independent components, spatial and temporal, *i.e.*,

$$x(y,t) = \chi(y)\phi(t). \quad (12)$$

The spatial component represents the mode shapes of the beam and time component is the harmonic oscillations. Therefore, the total solution is the superposition of the motion of each natural mode $\chi_n(y)$ of the beam,

$$x(y,t) = \sum_{n=1}^{\infty} \chi_n(y)\phi_n(t), \quad (13)$$

where n indexes the modes and $\phi_n(t)$ comprises of the harmonic oscillations of the natural modes. The solutions to $\chi_n(y)$ and $\phi_n(t)$ depend on the boundary and initial conditions for the beam, respectively [28].

To relate the strain to the transverse displacement of the beam, consider that the tensile stress, σ, at a point of the beam is equal to $-\frac{Mc}{I}$, where c is the distance from the point to the neutral axis. Hence from Hooke's Law,

$$E\epsilon = \sigma = -\frac{Mc}{I} = -Ec\frac{\partial^2 x(y)}{\partial y^2}. \quad (14)$$

Therefore the strain at the surface of the beam is related to displacement by

$$\epsilon(y,t) = -\frac{h}{2}\frac{\partial^2 x(y,t)}{\partial y^2} = -\frac{h}{2}\frac{\partial^2 \chi_n(y)}{\partial y^2}\phi_n(t). \quad (15)$$

Assuming the motion of the beam can be approximated by a finite number of modes, $\frac{\partial^2 \chi_n(y)}{\partial y^2}$ can be calculated, allowing for the solutions of $\phi_n(t)$ given the strain measurements $\epsilon(y,t)$. Finally, the displacement $x(y,t)$ is found by Eq. (13).

C. Control Hardware Design and Dynamics Model

A custom voltage/current amplifier is developed to control the bending motion of the IPMC actuator. Figure 6 shows the circuit block diagram and fabricated circuit board for the amplifier[1]. The amplifier is a class-B, emitter-follower design with feedback to minimize cross-over distortion [29]. In voltage mode, the voltage difference across the electrodes of the actuator is used in the feedback loop as shown in Fig. 6(a). The measured unloaded bandwidth (-3.01 dB) in voltage mode exceeds 100 kHz. Likewise, the measured cross-over distortion at different input frequencies for a 4 Ω resistive load is listed in Table I. In current mode, resistor R_s (1 Ω, 5 W) functions as a current sensor.

TABLE I
MEASURED AMPLIFIER CROSS-OVER DISTORTION WITH 4-Ω RESISTIVE LOAD AND TRIANGLE REFERENCE INPUT SIGNAL WITH 1 V AMPLITUDE.

Frequency (Hz)	Max. error (mV)	Max. error (%)
100	4	0.2
1000	40	2.0
10,000	162	8.1

A linear dynamics model is obtained by curve-fitting the measured frequency response of the IPMC actuator, where

[1]Circuit diagram is available by contacting the corresponding author.

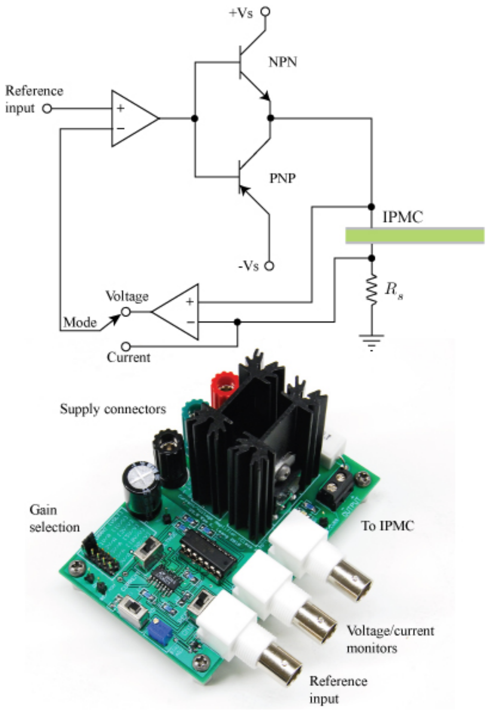

Fig. 6. Custom-design voltage/current amplifier for IPMC actuator: (a) circuit diagram and (b) fabricated circuit board.

the model is given by the following transfer function

$$G(s) = k_0 \frac{\omega_n^2}{s^2 + 2\xi\omega_n s + \omega_n^2} \left(\frac{a}{s+a} \right), \tag{16}$$

with $k_0 = 0.498$, $\zeta = 0.085$, $\omega_n = 88.907$ rad/s, and $a = 125$. A discrete time model $G(z)$ is created using Matlab's '`c2d`' command with a sampling period of $T = 1$ ms for designing the controllers in discrete time.

IV. EXPERIMENTAL RESULTS AND DISCUSSION

The repetitive controller is first simulated in the Matlab Simulink software, where the system is represented by a second-order linear dynamics model $G(s)$ to determine the controller parameters prior to implementation. The RC parameters are chosen as $k_{rc} = 1.0$, N = 2000, and m = 6 based on the discussion in Section II. For robustness, a low-pass filter $Q(z)$ with a cut-off frequency of 5 Hz is chosen. The controller was implemented using Matlab xPC Target environment using the sampling rate of 1 kHz. Sine and triangle reference inputs at 0.5, 1.0, 1.5, and 2.0 Hz are investigated.

For comparison, a discrete-time proportional-integral-derivative (PID) controller is designed with gains k_p = 1.5, $k_i = 9$, and $k_d = 0.0005$, and closed-loop sampling frequency of 1 kHz. The tip displacement is obtained using Eq. (13), with the assumption that the first mode of vibration models the bending motion.

The measured tracking results (strain sensor signal) and the tracking error at 0.5 Hz are shown in Fig. 7. Table II lists the maximum (e_{max}) and root-mean-squared (e_{rms}) tracking error for 0.5, 1.0, 1.5, and 2.0 Hz, computed as a percentage of the total output range.

With the PID controller, the maximum tracking error for the sine and triangle reference trajectories are relatively large; for example they exceed 10% at 1 Hz and above. However, by applying the RC, the measured tracking error is reduced significantly; for example at 0.5 Hz the maximum error with RC is 3.4% ($e_{rms} = 1.4\%$), over 55% lower compared to the PID controller. It is pointed out that because the RC is designed around a one-period delay, the controller begins to take effect after the first period. Compared to the PID controller, the tracking error for the RC diminishes with each operating period, where steady state is achieved after approximately 3 cycles (Fig. 7). Additional improvement in the tracking precision can be achieved by integrating the PID controller with RC, that is, replacing k_{rc} with a PID control block to further enhance closed-loop performance. Likewise, an internal feedback loop can also be used to account for unmodeled dynamics such as the slow back-relaxation effect.

In summary, the measured response shows that RC can be employed for tracking oscillatory reference trajectories in IPMCs for underwater applications. One unique advantage of the proposed sensing scheme is compactness. The strain sensor can be bonded to the surface of the IPMC or embedded within the polymer material. By incorporating additional sensors arranged in appropriate orientations, both bending and twisting behavior can be measured and subsequently used as feedback information.

V. CONCLUSIONS

This paper discussed the design of a discrete-time repetitive controller for tracking period reference trajectories in IPMC actuators used for underwater applications. The stability of the controller was analyzed in the discrete-time domain. The RC was applied to a newly fabricated perfluorinated ion exchange membrane based IPMC actuator with lithium as its counter-ion. The displacement of the IPMC actuator was measured by a strain gage sensor bonded to the surface of the IPMC actuator. The sensor is low cost, practical, effective, and importantly, compact. Tracking results show the combined control and sensing scheme can minimize the tracking error by approximately 50% compared to PID control for tracking of periodic signals including sinusoidal and triangular wave forms.

REFERENCES

[1] M. Shahinpoor and K. J. Kim, "Ionic polymer-metal composites: IV. industrial and medical applications," *Smart Mater. Struct.*, vol. 14, no. 1, pp. 197 – 214, 2005.

[2] K. Krishen, "Space applications for ionic polymer-metal composite sensors, actuators, and artificial muscles," *Acta Astronautica*, vol. 64, no. 11 – 12, pp. 1160 –1166, 2009.

[3] B.-K. Fang, M.-S. Ju, and C.-C. K. Lin, "A new approach to develop ionic polymer-metal composites (IPMC) actuator: fabrication and control for active catheter systems," *Sensors and Actuators A: Physical*, vol. 137, no. 2, pp. 321 – 329, 2007.

[4] E. Biddiss and T. Chau, "Electroactive polymeric sensors in hand prostheses: Bending response of an ionic polymer metal composite," *Medical Engineering and Physics*, vol. 28, no. 6, pp. 568 – 578, 2006.

[5] K. J. Kim, W. Yim, J. W. Paquette, and D. Kim, "Ionic polymer-metal composites for underwater operation," *J. of Intelligent Material Systems and Structures*, vol. 18, no. 2, pp. 123 – 131, 2007.

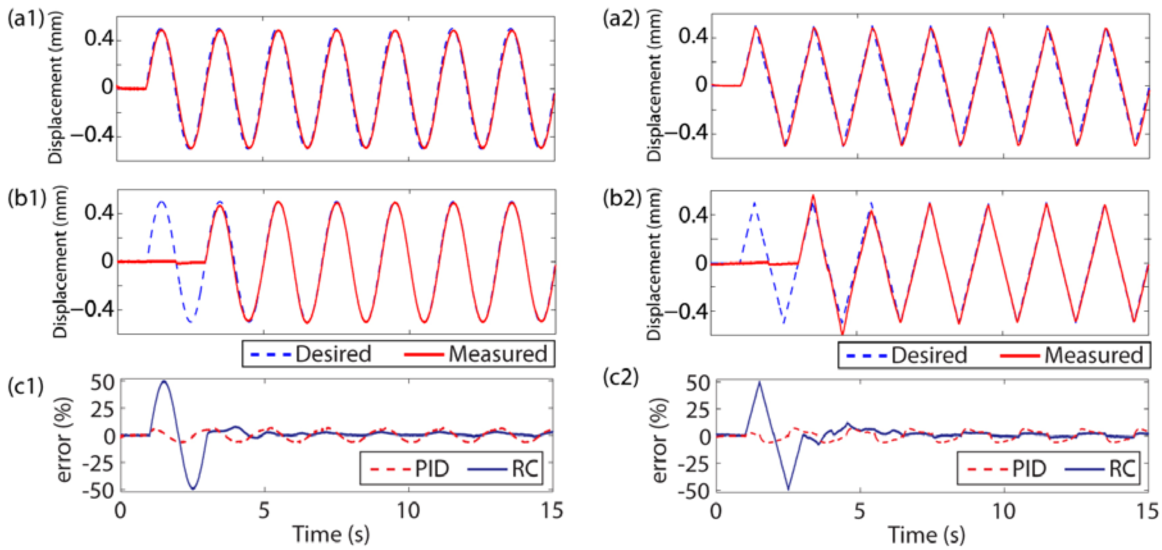

Fig. 7. Tracking results (0.5 Hz): sine-wave tracking using (a1) PID and (b1) RC; triangle-wave tracking using (a2) PID and (b2) RC; (c1) sine-wave tracking error and (c2) triangle-wave tracking error for PID and RC.

TABLE II
COMPARISON OF TRACKING PERFORMANCE BETWEEN PID AND RC FOR IPMC.

		0.5 Hz		1.0 Hz		1.5 Hz		2.0 Hz	
Cont.	**Traj.**	e_{max} **(%)**	e_{rms} **(%)**	e_{max} **(%)**	e_{rms} **(%)**	e_{max} **(%)**	e_{rms} **(%)**	e_{max} **(%)**	e_{rms} **(%)**
PID	Sine	7.6	4.4	11.1	6.7	14.9	9.6	17.0	11.1
PID	Triangle	7.5	4.3	11.4	7.5	15.1	10.1	17.2	11.6
RC	Sine	3.4	1.4	5.9	3.4	8.5	5.4	12.4	7.9
RC	Triangle	3.6	1.5	6.0	3.6	8.7	5.8	12.8	8.9

[6] M. Yamakita, A. Sera, N. Kamamichi, K. Asaka, and Z.-W. Luo, "A snake-like swimming robot using IPMC actuator/sensor," in *IEEE Intern. Conf. on Robotics and Automation*, Orlando, FL, 2006, pp. 1812 – 1817.

[7] S. Guo, Y. Ge, L. Li, and S. Liu, "Underwater swimming micro robot using IPMC actuator," in *Proc. of the 2006 IEEE Intern. Conf. on Mechatronics and Automation, June 25 - 28*, Luoyang, China, 2006, pp. 249 – 254.

[8] H. Nakadoi, D. Sobey, M. Yamakita, and T. Mukai, "Liquid environment-adaptive IPMC fish-like robot using extremum seeking feedback," in *IEEE/RSJ Intern. Conf. on Intelligent Robots and Systems (IROS)*, Nice, France, 2008.

[9] S. Guo, L. Shi, X. Ye, and L. Li, "A new jellyfish type of underwater microrobot," in *Proc. IEEE Intern. Conf. on Mechatronics and Automation*, Harbin, China, 2007, pp. 509 – 514.

[10] X. Tan, D. Kim, N. Usher, D. Laboy, J. Jackson, A. Kapetanovic, J. Rapai, B. Sabadus, and X. Zhou, "An autonomous robotic fish for mobile sensing," in *Proc. of the 2006 IEEE/RSJ Intern. Conf. on Intelligent Robots and Systems*, Beijing, China, 2006, pp. 5424 – 5429.

[11] A. Menozzi, H. A. Leinhos, D. N. Beal, and P. R. Bandyopadhyay, "Open-loop control of a multifin biorobotic rigid underwater vehicle," *IEEE J. Oceanic Engineering*, vol. 33, no. 2, pp. 59 – 68, 2008.

[12] P. R. Bandyopadhyay, D. N. Beal, and A. Menozzi, "Biorobotic insights into how animals swim," *J. of Experimental Biology*, vol. 211, pp. 206 – 214, 2008.

[13] Z. Chen, Y. Shen, N. Xi, and X. Tan, "Integrated sensing for ionic polymer–metal composite actuators using PVDF thin films," *Smart Mater. Struct.*, vol. 16, no. S262 – S271, 2007.

[14] C. Bonomo, L. Fortuna, P. Giannone, and S. Graziani, "A method to characterize the deformation of an ipmc sensing membrane," *Sensors and Actuators A: Physical*, vol. 123 – 124, pp. 146 – 154, 2005.

[15] Y. Shan and K. K. Leang, "Frequency-weighted feedforward control for dynamic compensation in ionic polymer-metal composite actuators," *Smart Mater. Struct.*, vol. 18, no. 12, p. 125016 (11 pages), 2009.

[16] B. C. Lavu, M. P. Schoen, and A. Mahajan, "Adaptive intelligent control of ionic polymermetal composites," *Smart Mater. Struct.*, vol. 14, pp. 466 – 474, 2005.

[17] K. Tsiakmakis, J. Brufau, M. Puig-Vidal, and T. Laopoulos, "Modeling IPMC actuators for model reference motion control," in *IEEE Proc. on Instrumentation and Measurement Technology*, Victoria, Vancouver Island, Canada, 2008.

[18] H.-H. Lin, B.-K. Fang, M.-S. Ju, and C.-C. K. Lin, "Control of ionic polymer-metal composites for active catheter systems via linear parameter-varying approach," *J. of Intelligent Material Systems and Structures*, vol. 20, no. 3, pp. 273 – 282, 2009.

[19] Z. Chen, K. Ki-Yong, and X. Tan, "Integrated IPMC/PVDF sensory actuator and its validation in feedback control," *Sensors and Actuators A, Physical*, vol. 144, no. 2, pp. 231 – 241, 2008.

[20] T. Inoue, M. Nakano, and S. lwai, "High accuracy control of a proton synchrotron magnet power supply," in *Proc. 8th World Congr. IFAC*, 1981, pp. 216 – 221.

[21] S. Hara, Y. Yamamoto, T. Omata, and M. Nakano, "Repetitive control system: a new type servo system for periodic exogenous signals," *IEEE Trans. Autom. Cont.*, vol. 33, no. 7, pp. 659 – 668, 1988.

[22] K. K. Chew and M. Tomizuka, "Digital control of repetitive errors in disk drive systems," *IEEE Cont. Syst. Mag.*, vol. 10, no. 1, pp. 16 – 20, 1990.

[23] M. Tomizuka, "Zero-phase tracking algorithm for digital control," *ASME J. Dyn. Syst. Meas. and Cont.*, vol. 109, pp. 65 – 68, 1987.

[24] K. Zhou and J. C. Doyle, *Essentials of robust control*. Prentice-Hall, Inc., 1998.

[25] H. L. Broberg and R. G. Molyet, "A new approach to phase cancellation in repetitive control," in *IEEE Industry Applications Society Annual Meeting*, vol. 3, 1994, pp. 1766 – 1770.

[26] R. O. Riddle, Y. Jung, S.-M. Kim, S. Song, B. Stolpman, K. J. Kim, and K. K. Leang, "Sectored-electrode IPMC actuator for bending and twisting motion," in *SPIE Smart Structures and Materials and Nondestructive Evaluation and Health Monitoring*, San Diego, CA, USA, 2010.

[27] A. C. Pisoni, C. Santolini, D. E. Hauf, and S. Dubowsky, "Displacements in a vibrating body by strain gauge measurements," in *Proc. of the 13th Intern. Conf. on Modal Analysis*, 1995.

[28] D. Inman, *Engineering vibration*, 2nd ed. Upper Saddle River, New Jersey: Prentice Hall, 2001.

[29] P. Horowitz and W. Hill, *The art of electronics*, 2nd ed. New York: Cambridge University Press, 1989.